Curie Temperature and Hopkinson Effect in Twin Roller Melt Spun Ni_2MnGa Shape Memory Alloys

Gabriela Pozo López[1,2], Luis M. Fabietti[1,2], Adriana M. Condó[3,4,5], Elin Winkler[3,4,5], Rafael N. Giordano[1], Néstor Haberkorn[3,5], and Silvia E. Urreta[1]

[1]Facultad de Matemática, Astronomía y Física, Universidad Nacional de Córdoba, Ciudad Universitaria, 5000 Córdoba, Argentina
[2]Instituto de Física Enrique Gaviola-CONICET, Argentina
[3]Centro Atómico Bariloche, Comisión Nacional de Energía Atómica, 8400 San Carlos de Bariloche, Argentina
[4]Instituto Balseiro, Universidad Nacional de Cuyo, 8400 San Carlos de Bariloche, Argentina
[5]Consejo Nacional de Investigaciones Científicas y Técnicas (CONICET), Argentina

The temperature dependence of the magnetic polarization near the Curie temperature T_C in Ni_2MnGa stoichiometric alloys, directly processed from the melt in a twin-roller melt-spinning device, is investigated. The effect of the solidification rate on the Hopkinson peak detected is evaluated in samples quenched at three different tangential wheel speeds of 10, 15, and 20 m/s. The resulting microstructures were previously characterized by X-ray diffraction (XRD), scanning electron microscopy (SEM), energy dispersive X-ray spectroscopy (EDS) and by transmission electron microscopy (TEM). EDS results indicated that all the alloys have the composition Ni_2MnGa; at room temperature and above this temperature, a cubic $L2_1$ ferromagnetic ordered austenitic phase is observed. The Curie temperatures and the magnitude of the Hopkinson effect are estimated from the magnetic polarization versus temperature curves measured in a Faraday balance, in the range 300 K–400 K. As expected for samples with identical composition, the Curie temperatures remain insensitive to the processing route. At low fields (10 mT), the magnitude of the Hopkinson effect is larger in samples quenched at lower rates and it practically vanishes in all the alloys for applied fields near 100 mT.

Index Terms—**Hopkinson effect, Ni_2MnGa, shape memory alloys, twin roller melt spinning.**

I. Introduction

UPON cooling from the melt, the Ni_2MnGa alloy undergoes multiple phase transformations [1], such as an ordering transition (from B2 to $L2_1$ order), a ferromagnetic phase transformation near 370 K and also a premartensitic and a martensitic transformation below room temperature. The phenomenon of ferromagnetic shape memory in Ni_2MnGa alloys, leading to large magnetic field-induced strains (MFIS), was first reported by Ullakko *et al.* in 1996 [2]; due to this property, these ferromagnetic alloys are active materials which may undergo relatively large strains by the motion of twin boundaries in the magnetic martensitic phase. Because of their high potential in the design of actuating devices and sensors [3], [4], they have been largely investigated [5]–[10].

The magnetoplastic strains solely produced by magnetic forces at constant temperature, with no mechanical bias stress, are negligibly small in polycrystalline alloys, as compared to those found in single crystals. In other words, MFIS is not reversible in polycrystals, except perhaps in those processed by melt spinning. Compared to the as-cast master alloy, the as-quenched melt spun ribbons exhibit a lower martensitic transformation temperature and Curie temperature T_C, and a reduced saturation polarization J_S; they also show marked steps in the $M(H)$ hysteresis loops [11], which have been attributed to magnetic field induced twin boundary motion (MFITBM), in the particular scenario of quenched-in internal stresses built up during solidification onto the rotating copper wheels.

The magnetic and the microstructure properties of Ni_2MnGa alloys, processed for the first time in a twin roller melt spinning device, have been recently reported [12] and the results compared with those obtained in samples solidified in a traditional single wheel melt spinning device. The former technique is known to impose a symmetric heat extraction during solidification, leading to high quenched-in stresses and an enhanced crystalline texture, as compared to conventional (single wheel) melt spinning. The alloys processed by this route also exhibit large and reversible MFIS, associated to a thermoelastic martensitic transformation at low temperature.

In this paper, we report further results concerning the Curie temperature and the magnetization behavior of Ni_2MnGa ribbons quenched at different rates in a twin roller melt spinning device. We focus on the magnetization behavior in the high temperature range, between room temperature and the Curie temperature T_C, where a Hopkinson peak has been reported [11], [13].

II. Experimental Procedure

A master alloy of nominal composition Ni_2MnGa was prepared by arc melting 99.9% Ni (Strem Chemicals), 99.95% Mn (Alfa Aesar) and 99.99% Ga (Strem Chemicals); the small ingots so obtained (about 5 g) were remelted four times to promote a homogeneous distribution of the components. All these procedures were conducted under a Zr gettered Ar atmosphere. The weight loss in the different ingots during arc melting was less than 0.3%. The alloy was further processed in a twin roller melt spinning device at three different tangential wheel speeds: 10,

Manuscript received February 16, 2013; revised March 20, 2013; accepted April 16, 2013. Date of current version July 23, 2013. Corresponding author: G. Pozo López (e-mail: gpozo@famaf.unc.edu.ar).

Color versions of one or more of the figures in this paper are available online at http://ieeexplore.ieee.org.

Digital Object Identifier 10.1109/TMAG.2013.2259617

TABLE I
TRANSFORMATION TEMPERATURES

Sample	I [K]	$M_S{}^S$ [K]	A_S [K]
V10	228	126	163
V15	231	123	146
V20	217	129	144

Transformation temperatures determined by electrical resistance measurements; I: premartensitic phase; M_s: onset of martensitic transformation (on cooling); A_S: onset of martensitic retransformation (on heating) [12].

15, and 20 m/s to obtain samples V10, V15, and V20, respectively. The springs forcing the contact between the two rolling wheels were set to 24 N. The alloy was obtained as ribbons of about 1–2 mm wide and 44–45 μm thick.

The resulting microstructures were characterized by X-ray diffraction (XRD), scanning electron microscopy (SEM) and transmission electron microscopy (TEM). XRD profiles were recorded in a Philips PW 1710/01 diffractometer in the 2θ range from 20° to 100°, in the Bragg-Brentano configuration, using Cu Kα radiation ($\lambda = 1.5418$ Å) and a graphite monochromator. Samples observed by TEM were thin foils prepared by twin-jet electropolishing with a 20% HNO_3 (nitric acid)/80% pro-analysis methanol electrolyte, at 12 V and 256 K. TEM observations and selected area electron diffraction patterns were performed in a Philips CM 200 UT microscope, operating at 200 kV and equipped with energy-dispersive X-ray spectroscopy (EDS) facility. A FEI Nova NanoSEM 230 was used to image the ribbon fracture surfaces.

Magnetic measurements were performed in 6-mm-long as-cast ribbons with the applied field parallel to the sample length; the small demagnetizing factors N obtained, 0.016 ± 0.002 (V10), 0.013 ± 0.002 (V15) and 0.012 ± 0.002 (V20), respectively, led to internal fields quite similar to the applied fields. A mean density of 8.134 g/cm^3 was assumed to calculate the magnetic polarization. The magnetic polarization as a function of field and temperature was measured in a Quantum Design SQUID magnetometer, under different applied fields, in the temperature range of 5 K–300 K. Curie temperatures were estimated from magnetization versus temperature curves measured in a Faraday balance, in the 300 K–400 K temperature range.

The premartensitic and martensitic transformation temperatures were detected by electrical resistance measurements with the conventional four-probe geometry between room temperature and 20 K and the results are listed in Table I [12].

III. RESULTS AND DISCUSSION

The resulting alloys are polycrystalline (Fig. 1), with small (4 μm) equiaxed grains near the surfaces and columnar grains 2–6 μm in diameter and 10–20 μm length, preferentially oriented normal to the ribbon plane. These columnar grains are longer and thicker in samples cooled at lower rates.

XRD (see Fig. 2) and electron diffraction studies [see Fig. 3(a)] indicate that the major phase at room temperature is the cubic $L2_1$ Ni_2MnGa ordered austenitic phase in all the samples.

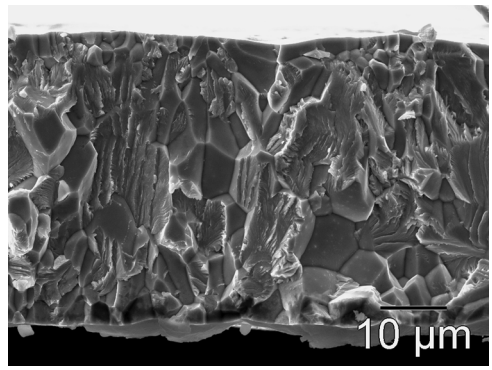

Fig. 1. SEM micrograph of the transversal section of a ribbon V15 showing small, equiaxed grains near the free surfaces and columnar grains inside.

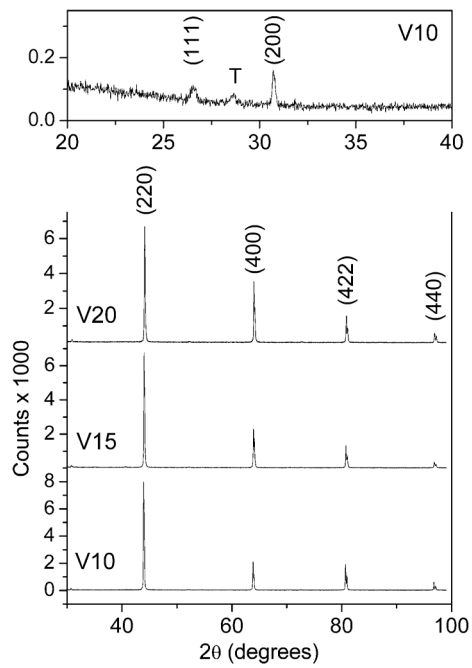

Fig. 2. XRD patterns of the alloys quenched at different substrate speeds, showing the fundamental diffraction lines from $L2_1$ austenitic phase. Superlattice diffraction lines (111) and (200) can be observed in the low angle region of the diffractograms. Letter "T" arises from the double-coated tape used to fix the ribbons to the holder.

The samples exhibit a pronounced crystallographic texture with the [100] direction perpendicular to the ribbon plane. Mn (S,Se) precipitates and dislocations are also observed [see Fig. 3(b) and 3(c)] embedded in the matrix, with mean precipitate size increasing as the quenching rate decreases.

During cooling below room temperature, the as-quenched alloys first present a premartensitic transformation to an intermediate cubic phase I at about 220 K–230 K depending on the quenching rate, and then a martensitic transformation starting at about 130 K.

The high temperature austenitic and the low temperature martensitic phases are ferromagnetic; in both cases the saturation polarization is lower in samples quenched at higher rates. Fig. 4 shows the hysteresis loops corresponding to the alloy quenched at different rates in both, the austenitic and the martensitic phases. In the austenitic phase, the samples exhibit very low coercivities, about 3 mT (V20) to 6 mT (V10). On the other hand, the demagnetization curves measured from

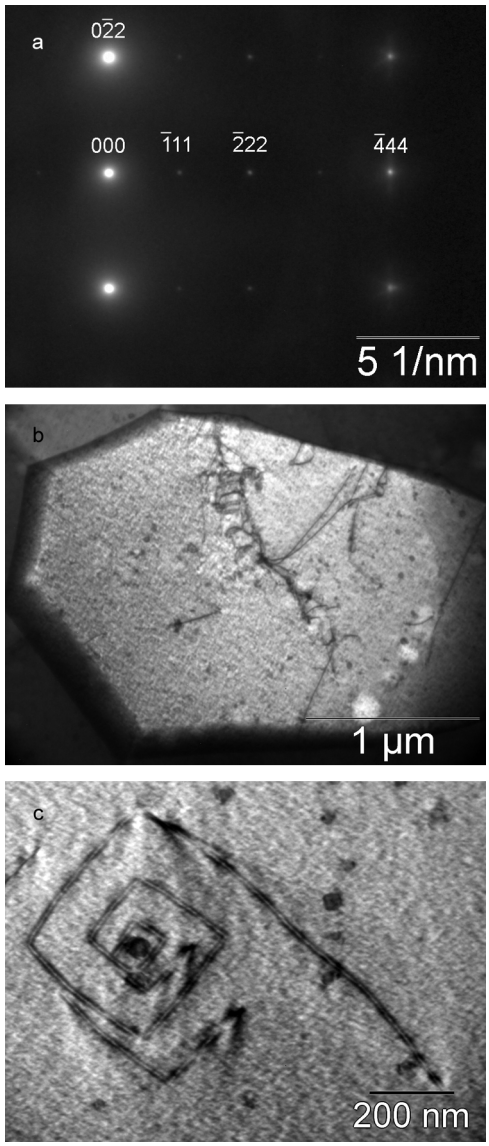

Fig. 3. TEM micrographs illustrating the microstructure of the austenitic phase. The sample is polycrystalline with a fcc Ni_2MnGa structure with $L2_1$ order. (a) Electron diffraction [211] zone axis pattern (V10). (b) Overview of the microstructure showing grain boundaries, Mn(Se,S) precipitates and dislocations (V10). (c) Detail of a helical dislocation around a precipitate (V15).

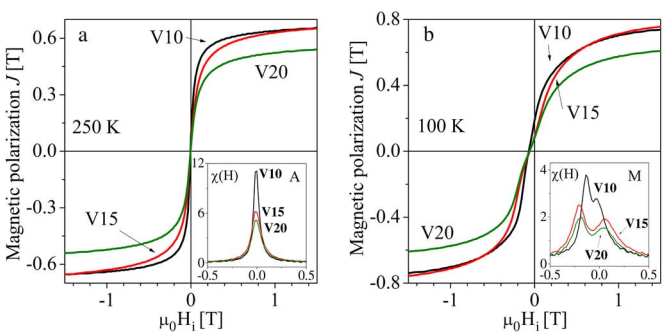

Fig. 4. Hysteresis loops of the alloy in the (a) austenitic phase and (b) in the martensitic phase showing the corresponding differential susceptibilities in the insets.

saturation in the martensitic state show two marked steps (better defined in the differential susceptibility shown in the insets of Fig. 4): a first one for positive fields in V15 and V10 (∼46 mT) and a larger second one for relatively large inverse fields (−130 mT to −250 mT) in all the samples. These steps are likely to arise [11]–[13] from a demagnetization mechanism involving field induced twin boundary motion in the few martensite variants selected by the crystallographic texture and the stresses built up in the ribbons during quenching.

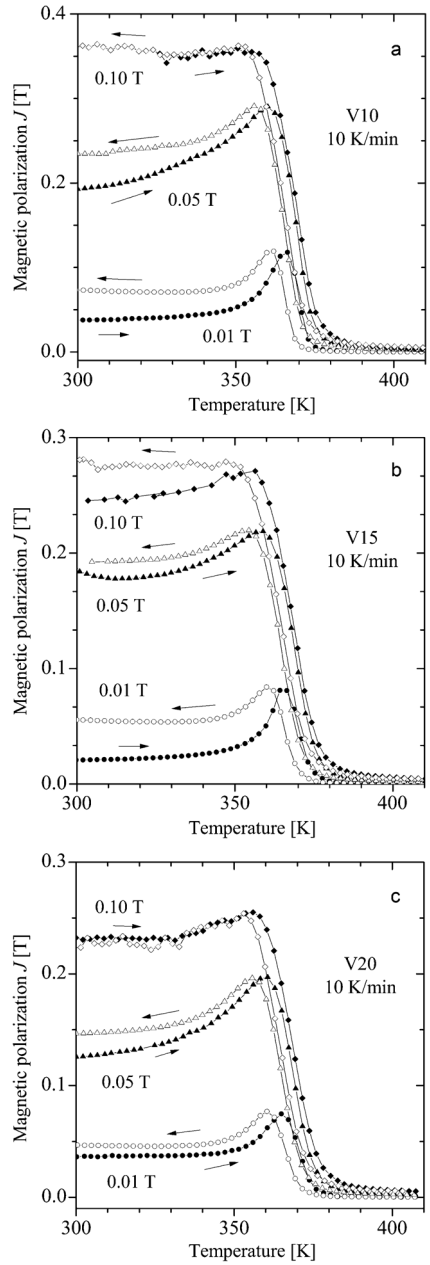

Fig. 5. Thermomagnetic heating and cooling curves, measured between 300 K and 400 K for the samples V10 (a), V15 (b) and V20 (c) to determine the corresponding Curie temperature. The Hopkinson effect takes place in all the alloys during cooling and heating curves.

The magnetization versus temperature curves measured under three external fields in the range between 300 K–400 K, during heating and the subsequent cooling, are shown in Fig. 5 for the three cooling rates investigated. The Curie temperatures T_C were calculated in the same way as those where the dJ/dT curves in Fig. 5 reach a minimum; the resulting values are quoted in Table II. It is observed that the Curie temperature does not depend on the sample microstructure as long as the

TABLE II
CURIE TEMPERATURE AND HOPKINSON EFFECT OF Ni_2MnGa ALLOYS

Field [T]	*0.01*	*0.05*	*0.1*	*0.01*
	T_C [K]	T_C [K]	T_C [K]	*HE* [%]
V10	371	369	371	12
V15	371	370	370	10
V20	371	369	369	8

Curie temperatures corresponding to the alloys quenched at different rates and measured at different external fields; they are estimated as the temperature where the curve dJ/dT reaches a minimum.

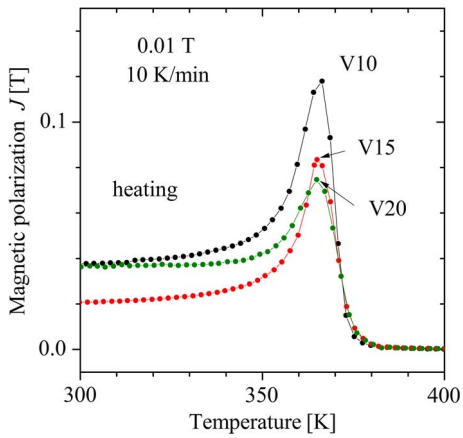

Fig. 6. Low field thermomagnetic curves measured during heating for the three samples investigated.

alloy composition remains unchanged. A Hopkinson peak [14] is clearly observed in all the alloys for the lower magnetic fields applied, but for fields of about 0.1 T this effect practically disappears in the three cases. The magnitude of the Hopkinson effect measured during heating and defined as $\mathrm{HE} = (J_{\mathrm{peak}} - J(300K))/J_S(300K)$ with J_{peak}, $J(300K)$ and $J_S(300K)$ the magnetic polarization at the peak, at 300 K and the saturation value at room temperature, respectively, are listed in Table II. The Hopkinson effect is observed because the crystal anisotropy constant K and the magnetostriction λ both decrease to zero at or below T_C. These two factors reduce the effectiveness of quenched residual microstresses, grain boundaries, antiphase boundaries and/or the Mn(S,Se) precipitates in hindering domain wall motion, leading to the polarization increment observed. For an applied field of 10 mT, the magnitude of the Hopkinson effect is larger in samples quenched at lower rates (see Fig. 6), in which the applied field is closer to the coercive field and further irreversible depinning events are expected when K and/or λ drop. In samples where the applied field is about three times the coercive field, irreversible magnetization orientation events are expected to be practically exhausted.

IV. CONCLUSION

Ni_2MnGa thin ribbons (40 μm thick) were produced by twin roller melt spinning at three different cooling rates. The effects of these quenching conditions on the austenitic phase magnetic polarization above room temperature and the Curie temperature have been investigated. The high temperature austenitic phase is ferromagnetic, with a Curie temperature of 370 $\pm$ 1 K, independent of the processing conditions.

Low field (10 mT) thermomagnetic curves show a Hopkinson peak, which practically disappear for fields of about 0.1 T. The magnitude of the Hopkinson effect is larger in samples quenched at low rates.

ACKNOWLEDGMENT

This work was supported in part by CONICET and SECyT-UNC.

REFERENCES

[1] A. N. Vasil'ev, A. D. Bozhko, V. V. Khovailo, I. E. Dikshtein, V. G. Shavrov, V. D. Buchelnikov, M. Matsumoto, S. Suzuki, T. Takagi, and J. Tani, "Structural and magnetic phase transitions in shape-memory alloys $Ni_{2+x}Mn_{1-x}Ga$," *Phys. Rev. B*, vol. 59, no. 2, pp. 1113–1120, 1999.

[2] K. Ullakko, J. K. Huang, C. Kantner, R. C. O'Handley, and V. V. Kokorin, "Large magnetic-field-induced strains in Ni_2MnGa single crystals," *Appl. Phys. Lett*, vol. 69, no. 13, pp. 1966–1968, 1996.

[3] R. Kainuma, Y. Imano, W. Ito, Y. Sutou, H. Morito, S. Okamoto, O. Kitakami, K. Oikawa, A. Fujita, T. Kanomata, and K. Ishida, *Nature*, vol. 439, pp. 957–960, 2006.

[4] D. C. Dunand and P. Müllner, "Size effects on magnetic actuation in Ni-Mn-Ga shape-memory alloy," *Adv. Mater.*, vol. 23, pp. 216–232, 2011.

[5] O. Söderberg, A. Sozinov, Y. Ge, S.-P. Hannula, and V. K. Lindroos, "Giant magnetostrictive materials," in *Handbook of Magnetic Materials*, K. H. J. Buschow, Ed. Amsterdam, The Netherlands: Elsevier Science, 2005, vol. 16.

[6] R. C. O'Handley and S. M. Allen, "Shape memory alloys, magnetically activated ferromagnetic shape memory materials," in *Encyclopedia of Smart Materials*. New York, NY, USA: Wiley, 2001, pp. 936–951.

[7] A. Vassil'ev, "Magnetic driven shape memory alloys," *J. Magn. Magn. Mater.*, vol. 242–245, pp. 66–67, 2002.

[8] B. Jiang, W. Zhou, Y. Liu, and X. Qi, "Recent progress of magnetically controlled shape memory materials," *Mater. Sci. Forum*, vol. 426–432, pp. 2285–2290, 2003.

[9] O. Heczko, "Magnetic shape memory effect and magnetization reversal," *J. Magn. Magn. Mater.*, vol. 290–291, pp. 787–794, 2005.

[10] J. Enkovaara, A. Ayuela, T. Zayak, P. Entel, L. Nordström, M. Dube, J. Jalkanen, J. Impola, and R. M. Nieminen, "Magnetically driven shape memory alloys," *Mater. Sci. Eng. A*, vol. 378, pp. 52–60, 2004.

[11] J. Wang, C. Jiang, R. Techapiesancharoenkij, D. Bono, S. M. Allen, and R. C. O'Handley, "Anomalous magnetizations in melt spinning Ni-Mn-Ga," *J. Appl. Phys.*, vol. 106, pp. 023923-1–023923-3, 2009.

[12] G. Pozo López, A. M. Condó, R. N. Giordano, S. E. Urreta, N. Haberkorn, E. Winkler, and L. M. Fabietti, "Microstructure and magnetic properties of as-cast Ni_2MnGa alloys processed by twin roller melt spinning," *J. Magn. Magn. Mater.* vol. 335, pp. 75–85, 2013.

[13] J. Wang, C. Jiang, R. Techapiesancharoenkij, D. Bono, S. M. Allen, and R. C. O'Handley, "Microstructure and magnetic properties of melt spinning Ni-Mn-Ga," *Intermetallics*, vol. 32, pp. 151–155, 2013.

[14] B. D. Cullity and C. D. Graham, *Introduction to Magnetic Materials*, 2nd ed. Piscataway, NJ, USA: IEEE Press, 2009, vol. 2, p. 323.